Biointerface Research in Applied Chemistry
Open-Access Journal (ISSN: 2069-5837)

Article
Volume 13, Issue 1, 2023, 66
https://doi.org/10.33263/BRIAC131.066

Computation of Reverse Degrees of Some Antiviral Drugs Targeting COVID 19 with QSPR Analysis

Parvez Ali [1,*], Syed Ajaz K. Kirmani [2], Alok Kumar [3]

[1] Department of Mechanical Engineering, College of Engineering, Qassim University, Unaizah, Saudi Arabia; parvezamu1@gmail.com (P.A.);
[2] Department of Electrical Engineering, College of Engineering, Qassim University, Unaizah, Saudi Arabia; ajazkirmani@gmail.com (S.A.K.K.);
[3] University Institute of Engineering and Technology, CSJM University, Kanpur, India; akumar.uiet@gmail.com (A.K.);
* Correspondence: p.ali@qu.edu.sa (P.A.), parvezamu1@gmail.com (P.A.);

Scopus Author ID 56158513100

Received: 23.11.2021; Accepted: 28.12.2021; Published: 2.02.2022

Abstract: COVID-19 has caused global disruptions infection. In the absence of a cure, the disease is still a cause for concern, so numerous research groups are focusing on identifying and developing new therapies to combat it. SARS-CoV-2, the virus responsible for the current epidemic, does not have specific antiviral drugs. Still, some antiviral drugs that target specific steps in their life cycle may prove effective in their treatment. It is advantageous to develop models based on the physicochemical properties of currently available antivirals. Therefore, this study determined QSPR models using reverse degree-based topological indices after analyzing the molecular structures of certain antiviral drugs. Firstly, we computed several reverse degree-based topological indices for these drugs, followed by a QSPR between the obtained reverse degree-based topological indices and various properties of these drugs. The study indicates that topological indices under investigation are directly associated with the physicochemical properties of the studied antiviral drugs.

Keywords: reverse degree indices; QSPR; COVID-19 drugs.

1. Introduction

Several outbreaks of SARS-CoV [1], H1N1 influenza [2], MERS-CoV [3], Ebola virus disease [4], and Zika virus [5] have taken place in the past two decades, and public health has become a concern because of these infections. In contrast to previous pandemics, COVID-19, which arises from the SARS-CoV-2 virus [6], is more infectious and lethal than previous viruses. The fight against SARS-CoV-2 requires effective therapies to treat infected people and prevent the global spread of this novel disease. As of now, a few COVID-19 vaccines [7] have demonstrated high effectiveness against the pandemic, but it is imperative to develop SARS-CoV-2 specific antiviral drugs in addition to effective vaccinations. The development of new antiviral drugs and the repurposing of existing antiviral drugs to combat COVID-19 is now a top priority for the global health community, so several antiviral drugs, including remdesivir, chloroquine and hydroxychloroquine, etc. [8–13], have been tested in vitro to inhibit SARS-CoV-2 infection and transmission. Clinical trials for SARS-CoV-2 failed to show a statistically significant effect of these drugs, possibly due to different pharmacological limitations that limit their efficacy [14,15]. As of yet, no specific antiviral drugs have been discovered to cure

COVID-19, so assessing the current antiviral drugs, as well as introducing new drugs, is pivotal at this point.

The discovery of a new chemical entity is a complex, expensive, and time-consuming process that ends with regulatory approval [16]. Iterative paradigms in the past had taken much time to synthesize compounds and to screen biologically, which required efficient data utilization, resulting in the need for lead compounds to be discovered effectively. Compound creation, synthesis, and biological screening using computer-aided drug design provide an alternative to traditional approaches, such as quantitative structure-activity relationships (QSARs) and quantitative structure-property relationships (QSPRs). Drug design is greatly facilitated by QSARs and QSPRs, which provide an alternative method of predicting the biological activity/molecular property of drug molecules that is affordable and faster [17,18]. A QSAR/QSPR model is based on molecular descriptors that are a numerical expression of the physical and chemical properties of the molecules [19–21]. Out of several descriptors, topological indices are the widely used descriptors in QSAR/QSPR derived from the topological (2D) representation of the molecular structure of a molecule[22]. To predict the boiling points of isomeric alkanes, Wiener proposed the first topological index to be used in QSPR modeling and named it the Wiener index [23,24]. In addition to the Wiener index, Zagreb and Randić are the two most widely used topological indices in QSPR modeling [25,26]. For more information on the topological indices, please refer to [27,28].

Many researchers are currently using topological indices to develop QSPR models that can be used to formulate drugs to combat the COVID-19 pandemic. Zhong *et al*.[29] established a QSPR for ev and ve-degree indices and found that the M^{ev} index and $M_1^{\beta ve}$ indexes are both useful indices to predict molecular weight and topological polar surface areas of phytochemicals studied against SARS-CoV-2 $3CL^{pro}$. Kirmani *et al*. [30] discovered that topological indices derived from M and NM-polynomial have a good predictive ability for the Arbidol, Chloroquine, Hydroxychloroquine, Lopinavir, Remdesivir, Ritonavir, Thalidomide, and Theaflavin drugs' physicochemical properties. Havare [31] developed multiple regression models for the antiviral drugs, including linear, quadratic, and cubic, based on degree, distance, and Mostar type topological indices.

The computation of different topological indices for drug molecules related to COVID-19 is another popular topic among researchers seeking to defeat the current pandemic. The topological index for Remdesivir was calculated using line graph concepts by Rosary [32] and para-line graphs by Liu [33]. Ahmed *et al*. [34] computed domination-based indices for the drugs chloroquine and hydroxychloroquine, whereas Jahanbani [35] obtained results based on general topological indices for the same drugs. Mondal *et al*. calculated multiplicative degree-based & multiplicative neighborhood degree sum-based indices for hydroxychloroquine, remdesivir, and theaflavin in [36], and the same authors provided M polynomial and NM polynomial with chloroquine added to the drug list [37]. The edge cut technique was utilized by Liu *et al*. [38] to generate distance-based and bond additive topological indices for 10 antiviral drugs used to combat the COVID-19 epidemic. Wei *et al*. [39] used a reverse degree-based topological indices approach, introduced by Kulli [40], to examine the molecular property of the Remdesivir drug deeply. Based on reverse degree, recently, Wei *et al*. [39] defined many reverse degree-based topological indices such as reverse first and second Zagreb, Randić, atom bond connectivity, geometric arithmetic, and reverse hyper Zagreb index.

2. Materials and Methods

In this article, we represent molecular graph by $\mathrm{G} = (\mathcal{V}, E)$ in which $\mathcal{V}(\mathrm{G})$ & $E(\mathrm{G})$ represent vertex & edge set and $|\mathcal{V}(\mathrm{G})|$ & $|E(\mathrm{G})|$ be the order and size of G. Let Φ_u denotes the degree of a vertex u and $\Delta(\mathrm{G})$ is the maximum degree of graph G. The reverse degree of a vertex u is defined as $R_u = \Delta(\mathrm{G}) - \Phi_u + 1$. Inspired by Wei *et al.*[39], we defined here reverse general inverse sum indeg index, denoted by $RG_{ISI_{(p,q)}}(G)$, and defined as:

$$RG_{ISI_{(p,q)}}(G) = \sum_{uv \in E(G)} [\Phi_u \Phi_v]^p \, [\Phi_u + \Phi_v]^q$$

where, p and q are some real numbers.

Table 1. Some reverse degree-based topological indices derived from reverse general inverse sum indeg index by assigning specific values to the parameters p and q.

(p, q)	$RG_{ISI_{(p,q)}}$	*Corresponding reverse topological index*
$(0,1)$	$RG_{ISI_{(0,1)}} = RM_1(G)$	Reverse first Zagreb index
$(1,0)$	$RG_{ISI_{(1,0)}} = RM_2(G)$	Reverse second Zagreb index
$\left(\frac{-1}{2}, 0\right)$	$RG_{ISI_{(\frac{-1}{2},0)}} = RR(G)$	Reverse Randić index
$\left(0, \frac{-1}{2}\right)$	$RG_{ISI_{(0,\frac{-1}{2})}} = RSCI(G)$	Reverse sum connectivity index
$(0,-1)$	$2RG_{ISI_{(0,-1)}} = RH(G)$	Reverse Harmonic index
$(0,2)$	$RG_{ISI_{(0,2)}} = RHZ(G)$	Reverse hyper Zagreb index
$\left(\frac{1}{2}, -1\right)$	$2RG_{ISI_{(\frac{1}{2},-1)}} = RGA(G)$	Reverse geometric arithmetic index
$\left(\frac{-1}{2}, 1\right)$	$\frac{1}{2}RG_{ISI_{(\frac{-1}{2},1)}} = RAG(G)$	Reverse arithmetic geometric index
$(1,-1)$	$RG_{ISI_{(1,-1)}} = RISI(G)$	Reverse inverse sum indeg index
$(-1,1)$	$RG_{ISI_{(-1,1)}} = RReZG_1(G)$	Reverse redefined first Zagreb index
$(1,1)$	$RG_{ISI_{(1,1)}} = RReZG_3(G)$	Reverse redefined third Zagreb index

In the next section of the paper, we provide a detailed description for obtaining an explicit expression for the reverse degree-based topological indices for the Arbidol, Camostat, Chloroquine, Hydroxychloroquine, Lopinavir, Nafamostat, Remdesivir, Ritonavir, Thalidomide, and Theaflavin drugs. We employed the edge partition, degree counting approach, and graph structure analysis to compute reverse degree-based topological indices for the molecular structure of the drugs under study also propose a predictive model (QSPR) based on reverse degree-based topological indices for the physicochemical properties of studied drugs.

3. Results and Discussion

In this article, the compounds Arbidol, Camostat, Chloroquine, Hydroxychloroquine, Lopinavir, Nafamostat, Remdesivir, Ritonavir, Thalidomide, and Theaflavin are represented by the letters *A*, *CA*, *C*, *H*, *L*, *N*, *Re*, *R*, *T*, and *TH* and their molecular graphs shown in Figures 1 to 10. The reverse edge partition for each molecular graph is also provided in each figure with their cardinalities. The reverse degree-based topological indices are now computed as follows:

Theorem 1: The reverse general inverse sum indeg index of Arbidol $RG_{ISI_{(p,q)}}(A)$ is given by,

$$RG_{ISI_{(p,q)}}(A) = (9)[1]^p[2]^q + (9)[2]^p[3]^q + (6)[3]^p[4]^q + (6)[4]^p[4]^q + (1)[6]^p[5]^q$$

Proof: By the graph structure analysis, the reverse degree-based edge partitions of the molecular structure of Arbidol are given in below Figure 1.

Chemical Structure (C22H25BrN2O3S) | Molecular Graph (A) | Reverse edge partitions & cardinalities

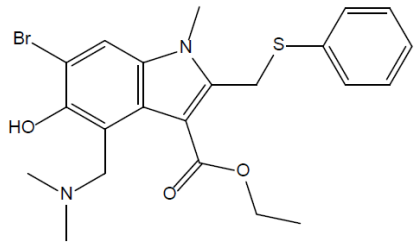

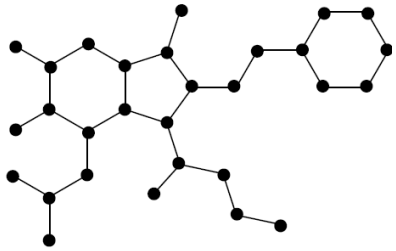

$E_1 = (\Phi_1, \Phi_1), |E_1| = 9$
$E_2 = (\Phi_1, \Phi_2), |E_2| = 9$
$E_3 = (\Phi_1, \Phi_3), |E_3| = 6$
$E_4 = (\Phi_2, \Phi_2), |E_4| = 6$
$E_5 = (\Phi_2, \Phi_3), |E_5| = 1$

Figure 1. Chemical and molecular graph of arbidol with edge partitions.

Now Applying the definition of reverse general inverse sum indeg index, $RG_{ISI_{(p,q)}}(A)$, we get

$$RG_{ISI_{(p,q)}}(A) = \sum_{uv \in E(A)} [\Phi_u \Phi_v]^p [\Phi_u + \Phi_v]^q$$

$$RG_{ISI_{(p,q)}}(A) = \sum_{uv \in E_1(A)} [\Phi_u \Phi_v]^p [\Phi_u + \Phi_v]^q + \sum_{uv \in E_2(A)} [\Phi_u \Phi_v]^p [\Phi_u + \Phi_v]^q$$

$$+ \sum_{uv \in E_3(A)} [\Phi_u \Phi_v]^p [\Phi_u + \Phi_v]^q + \sum_{uv \in E_4(A)} [\Phi_u \Phi_v]^p [\Phi_u + \Phi_v]^q + \sum_{uv \in E_5(A)} [\Phi_u \Phi_v]^p [\Phi_u + \Phi_v]^q$$

$$= |E_1(A)|[(1)(1)]^p[1+1]^q + |E_2(A)|[(1)(2)]^p[1+2]^q + |E_3(A)|[(1)(3)]^p[1+3]^q$$

$$+ |E_4(A)|[(2)(2)]^p[2+2]^q + |E_5(A)|[(2)(3)]^p[2+3]^q$$

$$= (9)[1]^p[2]^q + (9)[2]^p[3]^q + (6)[3]^p[4]^q + (6)[4]^p[4]^q + (1)[6]^p[5]^q$$

Hence the theorem.

From theorem 1 we have calculated exact values of some reverse degree-based indices of Arbidol as given below:

(i). $RG_{ISI_{(0,1)}} = RM_1(A) = 98$
(ii). $RG_{ISI_{(1,0)}} = RM_2(A) = 75$
(iii). $RG_{ISI_{(\frac{-1}{2},0)}} = RR(A) = 22.23631094$
(iv). $RG_{ISI_{(0,\frac{-1}{2})}} = RSCI(A) = 18.00732705$
(v). $2RG_{ISI_{(0,-1)}} = RH(A) = 21.40$
(vi). $RG_{ISI_{(0,2)}} = RHZ(A) = 334$
(vii). $2RG_{ISI_{(\frac{1}{2},-1)}} = RGA(A) = 29.66122969$
(viii). $\frac{1}{2}RG_{ISI_{(\frac{-1}{2},1)}} = RAG(A) = 32.49476550$
(ix). $RG_{ISI_{(1,-1)}} = RISI(A) = 22.20$
(x). $RG_{ISI_{(-1,1)}} = RReZG_1(A) = 46.33$
(xi). $RG_{ISI_{(1,1)}} = RReZG_3(A) = 270$

Theorem 2: The reverse general inverse sum indeg index of Camostat $RG_{ISI_{(p,q)}}(CA)$ is,

$$RG_{ISI_{(p,q)}}(CA) = (2)[1]^p[2]^q + (16)[2]^p[3]^q + (7)[3]^p[4]^q + (5)[4]^p[4]^q$$

Proof: Figure 2 shows the reverse degree-based edge partitions of Camostat's molecular structure as determined by graph structure analysis.

Chemical Structure ($C_{20}H_{22}N_4O_5$) | Molecular Graph (*CA*) | Reverse edge partitions & cardinalities

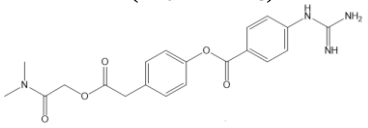

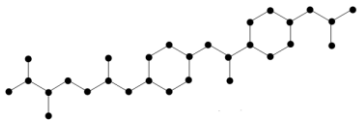

$E_1 = (\Phi_1, \Phi_1), |E_1| = 2$
$E_2 = (\Phi_1, \Phi_2), |E_2| = 16$
$E_3 = (\Phi_1, \Phi_3), |E_3| = 7$
$E_4 = (\Phi_2, \Phi_2), |E_4| = 5$

Figure 2. Chemical and molecular graph of camostat with edge partitions.

Applying the definition of $RG_{ISI_{(p,q)}}(CA)$, we have

$$RG_{ISI_{(p,q)}}(CA) = \sum_{uv\in E(CA)} [\Phi_u\Phi_v]^p\,[\Phi_u + \Phi_v]^q$$

$$RG_{ISI_{(p,q)}}(CA) = \sum_{uv\in E_1(CA)}[\Phi_u\Phi_v]^p\,[\Phi_u + \Phi_v]^q + \sum_{uv\in E_2(CA)}[\Phi_u\Phi_v]^p\,[\Phi_u + \Phi_v]^q + \sum_{uv\in E_3(CA)} [\Phi_u\Phi_v]^p\,[\Phi_u + \Phi_v]^q + \sum_{uv\in E_4(CA)} [\Phi_u\Phi_v]^p\,[\Phi_u + \Phi_v]^q$$

$$= |E_1(A)|[(1)(1)]^p[1+1]^q + |E_2(A)|[(1)(2)]^p[1+2]^q + |E_3(A)|[(1)(3)]^p[1+3]^q + |E_4(A)|[(2)(2)]^p[2+2]^q$$

$$= (2)[1]^p[2]^q + (16)[2]^p[3]^q + (7)[3]^p[4]^q + (5)[4]^p[4]^q$$

We determined the exact values of various reverse degree-based indices for Camostat drug-using theorem 2, as shown below:

(i). $RG_{ISI_{(0,1)}} = RM_1(CA) = 100$
(ii). $RG_{ISI_{(1,0)}} = RM_2(CA) = 75$
(iii). $RG_{ISI_{(\frac{-1}{2},0)}} = RR(CA) = 19.85516038$
(iv). $RG_{ISI_{(0,\frac{-1}{2})}} = RSCI(CA) = 16.65181787$
(v). $2RG_{ISI_{(0,-1)}} = RH(CA) = 18.66666667$
(vi). $RG_{ISI_{(0,2)}} = RHZ(CA) = 344$
(vii). $2RG_{ISI_{(\frac{1}{2},-1)}} = RGA(CA) = 28.14712250$
(viii). $\frac{1}{2}RG_{ISI_{(\frac{-1}{2},1)}} = RAG(CA) = 32.05346651$
(ix). $RG_{ISI_{(1,-1)}} = RISI(CA) = 21.91666667$
(x). $RG_{ISI_{(-1,1)}} = RReZG_1(CA) = 42.33333333$
(xi). $RG_{ISI_{(1,1)}} = RReZG_3(CA) = 264$

Theorem 3: The reverse general inverse sum indeg index of chloroquine $RG_{ISI_{(p,q)}}(C)$ is,

$$RG_{ISI_{(p,q)}}(C) = (2)[1]^p[2]^q + (12)[2]^p[3]^q + (2)[3]^p[4]^q + (5)[4]^p[4]^q + (2)[6]^p[5]^q$$

Proof: Figure 3 shows the reverse degree-based edge partitions of the molecular structure of chloroquine.

Chemical Structure ($C_{18}H_{26}ClN_3$) | Molecular Graph (C) | Reverse edge partitions & cardinalities

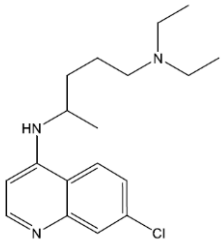

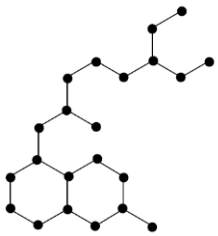

$E_1 = (\Phi_1, \Phi_1), |E_1| = 2$
$E_2 = (\Phi_1, \Phi_2), |E_2| = 12$
$E_3 = (\Phi_1, \Phi_3), |E_3| = 2$
$E_4 = (\Phi_2, \Phi_2), |E_4| = 5$
$E_5 = (\Phi_2, \Phi_3), |E_5| = 2$

Figure 3. Chemical and molecular graph of chloroquine with edge partitions.

Now Applying the definition of $RG_{ISI_{(p,q)}}(C)$, we get

$$RG_{ISI_{(p,q)}}(C) = \sum_{uv\in E(C)} [\Phi_u\Phi_v]^p\,[\Phi_u + \Phi_v]^q$$

$$RG_{ISI_{(p,q)}}(C) = \sum_{uv\in E_1(C)}[\Phi_u\Phi_v]^p\,[\Phi_u + \Phi_v]^q + \sum_{uv\in E_2(C)}[\Phi_u\Phi_v]^p\,[\Phi_u + \Phi_v]^q + \sum_{uv\in E_3(C)} [\Phi_u\Phi_v]^p\,[\Phi_u + \Phi_v]^q + \sum_{uv\in E_4(C)} [\Phi_u\Phi_v]^p\,[\Phi_u + \Phi_v]^q + \sum_{uv\in E_5(C)} [\Phi_u\Phi_v]^p\,[\Phi_u + \Phi_v]^q$$

$$= |E_1(A)|[(1)(1)]^p[1+1]^q + |E_2(A)|[(1)(2)]^p[1+2]^q + |E_3(A)|[(1)(3)]^p[1+3]^q + |E_4(A)|[(2)(2)]^p[2+2]^q + |E_5(A)|[(2)(3)]^p[2+3]^q$$

$$= (2)[1]^p[2]^q + (12)[2]^p[3]^q + (2)[3]^p[4]^q + (5)[4]^p[4]^q + (2)[6]^p[5]^q$$

Hence the theorem.

From theorem 3, some other reverse degree-based indices of Chloroquine are given below:

(i). $RG_{ISI_{(0,1)}} = RM_1(C) = 78$

(ii). $RG_{ISI_{(1,0)}} = RM_2(C) = 64$

(iii). $RG_{ISI_{(\frac{-1}{2},0)}} = RR(C) = 14.95647849$

(iv). $RG_{ISI_{(0,\frac{-1}{2})}} = RSCI(C) = 12.73684398$

(v). $2RG_{ISI_{(0,-1)}} = RH(C) = 14.30000000$

(vi). $RG_{ISI_{(0,2)}} = RHZ(C) = 278$

(vii). $2RG_{ISI_{(\frac{1}{2},-1)}} = RGA(C) = 22.00535110$

(viii). $\frac{1}{2}RG_{ISI_{(\frac{-1}{2},1)}} = RAG(C) = 24.07856459$

(ix). $RG_{ISI_{(1,-1)}} = RISI(C) = 17.90000000$

(x). $RG_{ISI_{(-1,1)}} = RReZG_1(C) = 31.33333333$

(xi). $RG_{ISI_{(1,1)}} = RReZG_3(C) = 240$

Theorem 4: The reverse general inverse sum indeg index of hydroxychloroquine $RG_{ISI_{(p,q)}}(H)$ is given by,

$$RG_{ISI_{(p,q)}}(H) = (2)[1]^p[2]^q + (12)[2]^p[3]^q + (2)[3]^p[4]^q + (6)[4]^p[4]^q + (2)[6]^p[5]^q$$

Proof: The reverse-degree edge partitions of the molecular structure of hydroxychloroquine are shown in Figure 4 by the graph structure analysis.

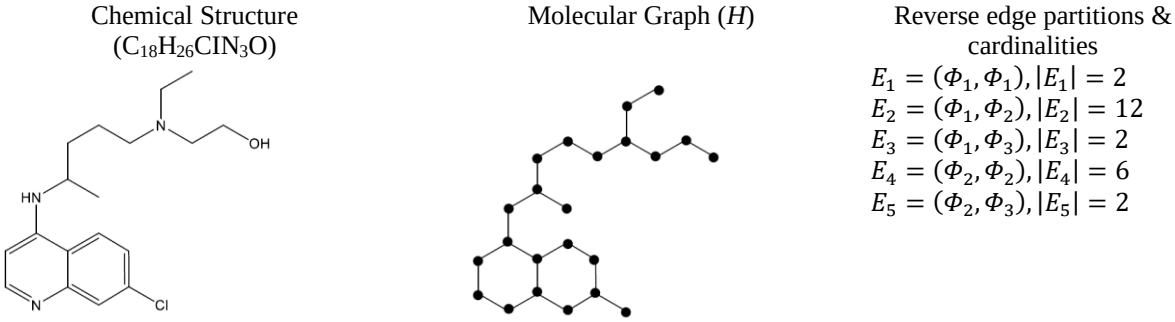

Figure 4. Chemical and molecular graph of hydroxychloroquine with edge partitions.

By the definition of, $RG_{ISI_{(p,q)}}(H)$, we have

$$RG_{ISI_{(p,q)}}(H) = \sum_{uv \in E(H)} [\Phi_u \Phi_v]^p [\Phi_u + \Phi_v]^q$$

$$RG_{ISI_{(p,q)}}(H) = \sum_{uv \in E_1(H)} [\Phi_u \Phi_v]^p [\Phi_u + \Phi_v]^q + \sum_{uv \in E_2(H)} [\Phi_u \Phi_v]^p [\Phi_u + \Phi_v]^q$$

$$+ \sum_{uv \in E_3(H)} [\Phi_u \Phi_v]^p [\Phi_u + \Phi_v]^q + \sum_{uv \in E_4(H)} [\Phi_u \Phi_v]^p [\Phi_u + \Phi_v]^q + \sum_{uv \in E_5(H)} [\Phi_u \Phi_v]^p [\Phi_u + \Phi_v]^q$$

$$= |E_1(A)|[(1)(1)]^p[1+1]^q + |E_2(A)|[(1)(2)]^p[1+2]^q + |E_3(A)|[(1)(3)]^p[1+3]^q$$

$$+|E_4(A)|[(2)(2)]^p[2+2]^q + |E_5(A)|[(2)(3)]^p[2+3]^q$$

$$= (2)[1]^p[2]^q + (12)[2]^p[3]^q + (2)[3]^p[4]^q + (6)[4]^p[4]^q + (2)[6]^p[5]^q$$

From theorem 4 the exact values of some reverse degree-based indices of hydroxychloroquine are:

(i). $RG_{ISI_{(0,1)}} = RM_1(H) = 82$

(ii). $RG_{ISI_{(1,0)}} = RM_2(H) = 68$

(iii). $RG_{ISI_{(\frac{-1}{2},0)}} = RR(H) = 15.45647849$

(iv). $RG_{ISI_{(0,\frac{-1}{2})}} = RSCI(H) = 13.23684398$

(v). $2RG_{ISI_{(0,-1)}} = RH(H) = 14.80000000$

(vi). $RG_{ISI_{(0,2)}} = RHZ(H) = 294$

(vii). $2RG_{ISI_{(\frac{1}{2},-1)}} = RGA(H) = 23.00535110$

(viii). $\frac{1}{2}RG_{ISI_{(\frac{-1}{2},1)}} = RAG(H) = 25.07856459$

(ix). $RG_{ISI_{(1,-1)}} = RISI(H) = 18.90000000$

(x). $RG_{ISI_{(-1,1)}} = RReZG_1(H) = 32.33333333$

(xi). $RG_{ISI_{(1,1)}} = RReZG_3(H) = 256$

Theorem 5: The reverse general inverse sum indeg index of lopinavir $RG_{ISI_{(p,q)}}(L)$ is,

$RG_{ISI_{(p,q)}}(L) = (7)[1]^p[2]^q + (20)[2]^p[3]^q + (8)[3]^p[4]^q + (14)[4]^p[4]^q$

Proof: In Figure 5, we present a reverse degree-based edge partitioning of the molecular structure of Lopinavir based on the structure analysis.

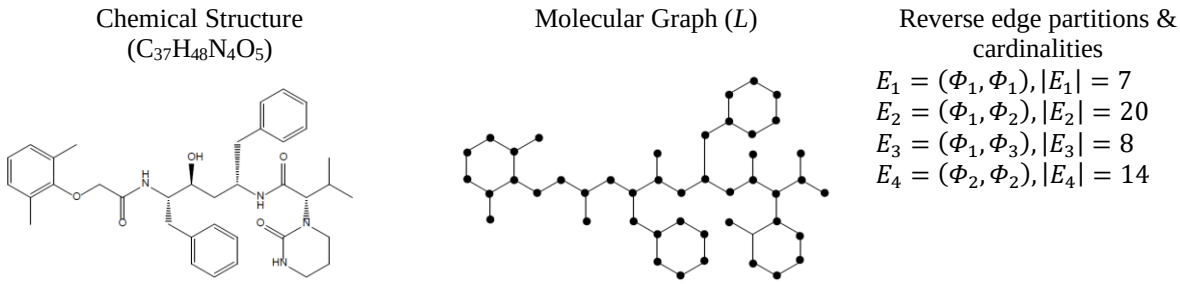

Figure 5. Chemical and Molecular Graph of Lopinavir with Edge Partitions.

Applying the definition of, $RG_{ISI_{(p,q)}}(L)$,

$$RG_{ISI_{(p,q)}}(L) = \sum_{uv\in E(L)} [\Phi_u\Phi_v]^p\,[\Phi_u + \Phi_v]^q$$

$$RG_{ISI_{(p,q)}}(L) = \sum_{uv\in E_1(L)}[\Phi_u\Phi_v]^p\,[\Phi_u + \Phi_v]^q + \sum_{uv\in E_2(L)}[\Phi_u\Phi_v]^p\,[\Phi_u + \Phi_v]^q + \sum_{uv\in E_3(L)} [\Phi_u\Phi_v]^p\,[\Phi_u + \Phi_v]^q + \sum_{uv\in E_4(L)} [\Phi_u\Phi_v]^p\,[\Phi_u + \Phi_v]^q$$

$$= |E_1(A)|[(1)(1)]^p[1+1]^q + |E_2(A)|[(1)(2)]^p[1+2]^q + |E_3(A)|[(1)(3)]^p[1+3]^q + |E_4(A)|[(2)(2)]^p[2+2]^q$$

$$= (7)[1]^p[2]^q + (20)[2]^p[3]^q + (8)[3]^p[4]^q + (14)[4]^p[4]^q$$

Hence the result.

Using theorem 5 we have some reverse degree-based indices of lopinavir as below:

(i). $RG_{ISI_{(0,1)}} = RM_1(L) = 162$

(ii). $RG_{ISI_{(1,0)}} = RM_2(L) = 127$

(iii). $RG_{ISI_{(\frac{-1}{2},0)}} = RR(L) = 32.76093778$

(iv). $RG_{ISI_{(0,\frac{-1}{2})}} = RSCI(L) = 27.49675286$

(v). $2RG_{ISI_{(0,-1)}} = RH(L) = 31.33333333$

(vi). $RG_{ISI_{(0,2)}} = RHZ(L) = 560$

(vii). $2RG_{ISI_{(\frac{1}{2},-1)}} = RGA(L) = 46.78438405$

(viii). $\frac{1}{2}RG_{ISI_{(\frac{-1}{2},1)}} = RAG(L) = 51.45080774$

(ix). $RG_{ISI_{(1,-1)}} = RISI(L) = 36.83333333$

(x). $RG_{ISI_{(-1,1)}} = RReZG_1(L) = 68.66666667$

(xi). $RG_{ISI_{(1,1)}} = RReZG_3(L) = 454$

Theorem 6: The reverse general inverse sum indeg index of nafamostat $RG_{ISI_{(p,q)}}(N)$ is,

$RG_{ISI_{(p,q)}}(N) = (3)[1]^p[2]^q + (16)[2]^p[3]^q + (5)[3]^p[4]^q + (4)[4]^p[4]^q$

Proof: Figure 6 shows the reverse degree-based edge partitions of nafamostat's molecular structure as determined by graph structure analysis.

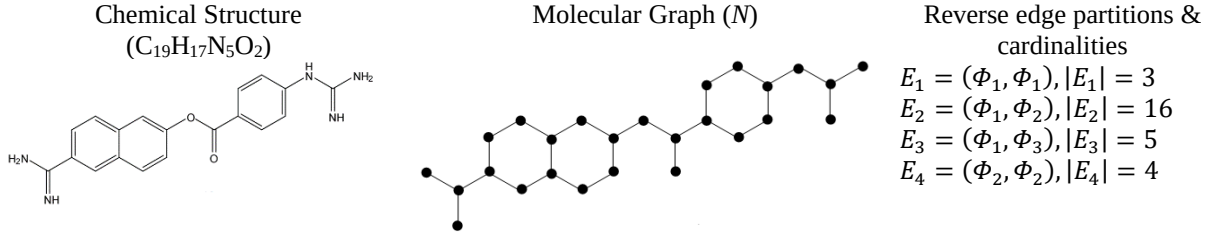

Figure 6. Chemical and molecular graph of nafamostat with edge partitions.

Applying the definition of $RG_{ISI_{(p,q)}}(N)$, we have

$$RG_{ISI_{(p,q)}}(N) = \sum_{uv\in E(N)} [\Phi_u\Phi_v]^p\,[\Phi_u+\Phi_v]^q$$

$$RG_{ISI_{(p,q)}}(N) = \sum_{uv\in E_1(N)}[\Phi_u\Phi_v]^p\,[\Phi_u+\Phi_v]^q + \sum_{uv\in E_2(N)}[\Phi_u\Phi_v]^p\,[\Phi_u+\Phi_v]^q + \sum_{uv\in E_3(N)} [\Phi_u\Phi_v]^p\,[\Phi_u+\Phi_v]^q + \sum_{uv\in E_4(N)} [\Phi_u\Phi_v]^p\,[\Phi_u+\Phi_v]^q$$

$$= |E_1(A)|[(1)(1)]^p[1+1]^q + |E_2(A)|[(1)(2)]^p[1+2]^q + |E_3(A)|[(1)(3)]^p[1+3]^q + |E_4(A)|[(2)(2)]^p[2+2]^q$$

$$= (3)[1]^p[2]^q + (16)[2]^p[3]^q + (5)[3]^p[4]^q + (4)[4]^p[4]^q$$

Hence the theorem.

We determined the exact values of various reverse degree-based indices for Nafamostat drug using theorem 6, as shown below:

(i). $RG_{ISI_{(0,1)}} = RM_1(N) = 90$

(ii). $RG_{ISI_{(1,0)}} = RM_2(N) = 66$

(iii). $RG_{ISI_{(\frac{-1}{2},0)}} = RR(N) = 19.20045985$

(iv). $RG_{ISI_{(0,\frac{-1}{2})}} = RSCI(N) = 15.85892465$

(v). $2RG_{ISI_{(0,-1)}} = RH(N) = 18.16666667$

(vi). $RG_{ISI_{(0,2)}} = RHZ(N) = 300$

(vii). $2RG_{ISI_{(\frac{1}{2},-1)}} = RGA(N) = 26.41507169$

(viii). $\frac{1}{2}RG_{ISI_{(\frac{-1}{2},1)}} = RAG(N) = 29.74406543$

(ix). $RG_{ISI_{(1,-1)}} = RISI(N) = 19.91666667$

(x). $RG_{ISI_{(-1,1)}} = RReZG_1(N) = 40.66666667$

(xi). $RG_{ISI_{(1,1)}} = RReZG_3(N) = 226$

Theorem 7: The reverse general inverse sum indeg index of Remdesivir $RG_{ISI_{(p,q)}}(Re)$ is,

$$RG_{ISI_{(p,q)}}(Re) = (2)[2]^p[3]^q + (5)[3]^p[4]^q + (1)[4]^p[5]^q + (6)[4]^p[4]^q + (14)[6]^p[5]^q + (5)[8]^p[6]^q + (9)[9]^p[6]^q + (3)[12]^p[7]^q$$

Proof: Figure 7 shows the reverse degree-based edge partitions of the molecular structure of remdesivir.

Chemical Structure ($C_{27}H_{35}N_6O_8P$)	Molecular Graph (*Re*)	Reverse edge partitions & cardinalities
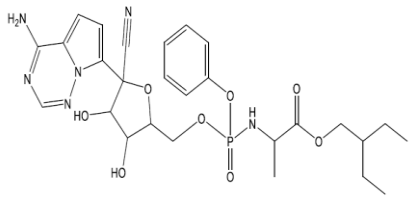	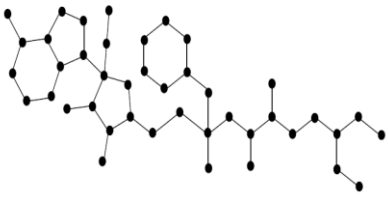	$E_1 = (\Phi_1, \Phi_2), \lvert E_1\rvert = 2$ $E_2 = (\Phi_1, \Phi_3), \lvert E_2\rvert = 5$ $E_3 = (\Phi_1, \Phi_4), \lvert E_3\rvert = 1$ $E_4 = (\Phi_2, \Phi_2), \lvert E_4\rvert = 6$ $E_5 = (\Phi_2, \Phi_3), \lvert E_5\rvert = 14$ $E_6 = (\Phi_2, \Phi_4), \lvert E_6\rvert = 5$ $E_7 = (\Phi_3, \Phi_3), \lvert E_7\rvert = 9$ $E_8 = (\Phi_3, \Phi_4), \lvert E_8\rvert = 3$

Figure 7. Chemical and molecular graph of remdesivir with edge partitions.

By, $RG_{ISI_{(p,q)}}(Re)$, we get

$$RG_{ISI_{(p,q)}}(Re) = \sum_{uv\in E(Re)} [\Phi_u\Phi_v]^p\,[\Phi_u+\Phi_v]^q$$

$$RG_{ISI_{(p,q)}}(Re) = \sum_{uv\in E_1(Re)}[\Phi_u\Phi_v]^p\,[\Phi_u+\Phi_v]^q + \sum_{uv\in E_2(Re)}[\Phi_u\Phi_v]^p\,[\Phi_u+\Phi_v]^q + \sum_{uv\in E_3(Re)} [\Phi_u\Phi_v]^p\,[\Phi_u+\Phi_v]^q + \sum_{uv\in E_4(Re)} [\Phi_u\Phi_v]^p\,[\Phi_u+\Phi_v]^q + \sum_{uv\in E_5(Re)} [\Phi_u\Phi_v]^p\,[\Phi_u+\Phi_v]^q + \sum_{uv\in E_6(Re)} [\Phi_u\Phi_v]^p\,[\Phi_u+\Phi_v]^q + \sum_{uv\in E_7(Re)} [\Phi_u\Phi_v]^p\,[\Phi_u+\Phi_v]^q + \sum_{uv\in E_8(Re)} [\Phi_u\Phi_v]^p\,[\Phi_u+\Phi_v]^q$$

$$= |E_1(A)|[(1)(2)]^p[1+2]^q + |E_2(A)|[(1)(3)]^p[1+3]^q + |E_3(A)|[(1)(4)]^p[1+4]^q$$

$$+|E_4(A)|[(2)(2)]^p[2+2]^q + |E_5(A)|[(2)(3)]^p[2+3]^q + |E_6(A)|[(2)(4)]^p[2+4]^q + |E_7(A)|[(3)(3)]^p[3+3]^q + |E_8(A)|[(3)(4)]^p[3+4]^q$$
$$= (2)[2]^p[3]^q + (5)[3]^p[4]^q + (1)[4]^p[5]^q + (6)[4]^p[4]^q + (14)[6]^p[5]^q + (5)[8]^p[6]^q + (9)[9]^p[6]^q + (3)[12]^p[7]^q$$

From theorem 7, some other reverse degree-based indices of remdesivir are given below:

(i). $RG_{ISI_{(0,1)}} = RM_1(Re) = 230$
(ii). $RG_{ISI_{(1,0)}} = RM_2(Re) = 288$
(iii). $RG_{ISI_{(\frac{-1}{2},0)}} = RR(Re) = 19.15023333$
(iv). $RG_{ISI_{(0,\frac{-1}{2})}} = RSCI(Re) = 20.21227396$
(v). $2RG_{ISI_{(0,-1)}} = RH(Re) = 18.35714286$
(vi). $RG_{ISI_{(0,2)}} = RHZ(Re) = 1220$
(vii). $2RG_{ISI_{(\frac{1}{2},-1)}} = RGA(Re) = 43.41616283$
(viii). $\frac{1}{2}RG_{ISI_{(\frac{-1}{2},1)}} = RAG(Re) = 46.76790298$
(ix). $RG_{ISI_{(1,-1)}} = RISI(Re) = 53.99285714$
(x). $RG_{ISI_{(-1,1)}} = RReZG_1(Re) = 40.08333333$
(xi). $RG_{ISI_{(1,1)}} = RReZG_3(Re) = 1586$

Theorem 8: The reverse general inverse sum indeg index of ritonavir $RG_{ISI_{(p,q)}}(R)$ is,

$$RG_{ISI_{(p,q)}}(R) = (5)[1]^p[2]^q + (26)[2]^p[3]^q + (9)[3]^p[4]^q + (13)[4]^p[4]^q$$

Proof: The reverse-degree edge partitions of the molecular structure of Ritonavir are shown in Figure 8 by the graph structure analysis.

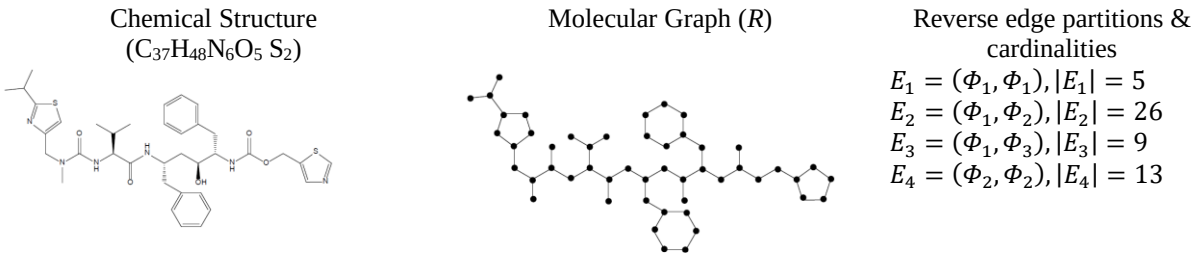

Figure 8. Chemical and molecular graph of ritonavir with edge partitions.

Applying the definition of $RG_{ISI_{(p,q)}}(R)$, we have

$$RG_{ISI_{(p,q)}}(R) = \sum_{uv \in E(R)} [\Phi_u \Phi_v]^p [\Phi_u + \Phi_v]^q$$
$$RG_{ISI_{(p,q)}}(R) = \sum_{uv \in E_1(R)} [\Phi_u \Phi_v]^p [\Phi_u + \Phi_v]^q + \sum_{uv \in E_2(R)} [\Phi_u \Phi_v]^p [\Phi_u + \Phi_v]^q + \sum_{uv \in E_3(R)} [\Phi_u \Phi_v]^p [\Phi_u + \Phi_v]^q + \sum_{uv \in E_4(R)} [\Phi_u \Phi_v]^p [\Phi_u + \Phi_v]^q$$
$$= |E_1(A)|[(1)(1)]^p[1+1]^q + |E_2(A)|[(1)(2)]^p[1+2]^q + |E_3(A)|[(1)(3)]^p[1+3]^q + |E_4(A)|[(2)(2)]^p[2+2]^q$$
$$= (5)[1]^p[2]^q + (26)[2]^p[3]^q + (9)[3]^p[4]^q + (13)[4]^p[4]^q$$

Hence the result.

From theorem 8 the exact values of some reverse degree-based indices of ritonavir are:

(i). $RG_{ISI_{(0,1)}} = RM_1(R) = 176$
(ii). $RG_{ISI_{(1,0)}} = RM_2(R) = 136$
(iii). $RG_{ISI_{(\frac{-1}{2},0)}} = RR(R) = 35.08092873$
(iv). $RG_{ISI_{(0,\frac{-1}{2})}} = RSCI(R) = 29.54664090$
(v). $2RG_{ISI_{(0,-1)}} = RH(R) = 33.33333333$
(vi). $RG_{ISI_{(0,2)}} = RHZ(R) = 606$
(vii). $2RG_{ISI_{(\frac{1}{2},-1)}} = RGA(R) = 50.30726371$
(viii). $\frac{1}{2}RG_{ISI_{(\frac{-1}{2},1)}} = RAG(R) = 55.96946931$
(ix). $RG_{ISI_{(1,-1)}} = RISI(R) = 39.58333333$
(x). $RG_{ISI_{(-1,1)}} = RReZG_1(R) = 74$
(xi). $RG_{ISI_{(1,1)}} = RReZG_3(R) = 482$

Theorem 9: The reverse general inverse sum indeg index of thalidomide $RG_{ISI_{(p,q)}}(T)$ is,

$$RG_{ISI_{(p,q)}}(T) = (7)[1]^p[2]^q + (6)[2]^p[3]^q + (4)[3]^p[4]^q + (4)[4]^p[4]^q$$

Proof: By the graph structure analysis, the reverse degree-based edge partitions of the molecular structure of thalidomide are given in below Figure 9.

Chemical Structure ($C_{13}H_{10}N_2O_4$)

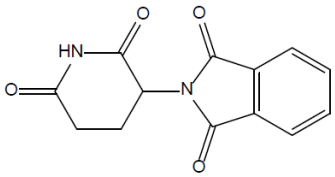

Molecular Graph (T)

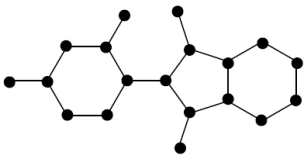

Reverse edge partitions & cardinalities

$E_1 = (\Phi_1, \Phi_1), |E_1| = 7$
$E_2 = (\Phi_1, \Phi_2), |E_2| = 6$
$E_3 = (\Phi_1, \Phi_3), |E_3| = 4$
$E_4 = (\Phi_2, \Phi_2), |E_4| = 4$

Figure 9. Chemical and molecular graph of thalidomide with edge partitions.

Now Applying the definition of reverse general inverse sum indeg index, $RG_{ISI_{(p,q)}}(T)$, we get

$$RG_{ISI_{(p,q)}}(T) = \sum_{uv \in E(T)} [\Phi_u \Phi_v]^p [\Phi_u + \Phi_v]^q$$

$$RG_{ISI_{(p,q)}}(T) = \sum_{uv \in E_1(T)} [\Phi_u \Phi_v]^p [\Phi_u + \Phi_v]^q + \sum_{uv \in E_2(T)} [\Phi_u \Phi_v]^p [\Phi_u + \Phi_v]^q + \sum_{uv \in E_3(T)} [\Phi_u \Phi_v]^p [\Phi_u + \Phi_v]^q + \sum_{uv \in E_4(T)} [\Phi_u \Phi_v]^p [\Phi_u + \Phi_v]^q$$

$$= |E_1(A)|[(1)(1)]^p[1+1]^q + |E_2(A)|[(1)(2)]^p[1+2]^q + |E_3(A)|[(1)(3)]^p[1+3]^q + |E_4(A)|[(2)(2)]^p[2+2]^q$$

$$= (7)[1]^p[2]^q + (6)[2]^p[3]^q + (4)[3]^p[4]^q + (4)[4]^p[4]^q$$

Hence the theorem.

From theorem 9 we have calculated exact values of some reverse degree-based indices of Thalidomide as given below:

(i). $RG_{ISI_{(0,1)}} = RM_1(T) = 64$

(ii). $RG_{ISI_{(1,0)}} = RM_2(T) = 47$

(iii). $RG_{ISI_{(\frac{-1}{2},0)}} = RR(T) = 15.55204177$

(iv). $RG_{ISI_{(0,\frac{-1}{2})}} = RSCI(T) = 12.41384908$

(v). $2RG_{ISI_{(0,-1)}} = RH(T) = 15$

(vi). $RG_{ISI_{(0,2)}} = RHZ(T) = 210$

(vii). $2RG_{ISI_{(\frac{1}{2},-1)}} = RGA(T) = 20.12095587$

(viii). $\frac{1}{2}RG_{ISI_{(\frac{-1}{2},1)}} = RAG(T) = 21.98276318$

(ix). $RG_{ISI_{(1,-1)}} = RISI(T) = 14.50000000$

(x). $RG_{ISI_{(-1,1)}} = RReZG_1(T) = 32.33333333$

(xi). $RG_{ISI_{(1,1)}} = RReZG_3(T) = 162$

Theorem 10: The reverse general inverse sum indeg index oftheaflavin $RG_{ISI_{(p,q)}}(TH)$ is,

$$RG_{ISI_{(p,q)}}(TH) = (14)[1]^p[2]^q + (22)[2]^p[3]^q + (10)[3]^p[4]^q$$

Proof: In Figure 10, we present a reverse degree-based edge partitioning of the molecular structure of theaflavin based on the structure analysis.

Chemical Structure ($C_{29}H_{24}O_{12}$)

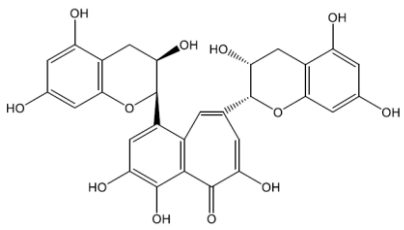

Molecular Graph (TH)

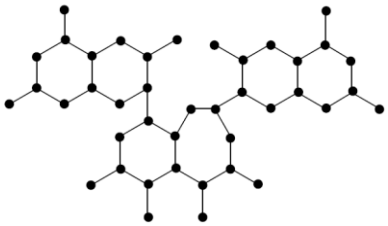

Reverse edge partitions & cardinalities

$E_1 = (\Phi_1, \Phi_1), |E_1| = 14$
$E_2 = (\Phi_1, \Phi_2), |E_2| = 22$
$E_3 = (\Phi_1, \Phi_3), |E_3| = 10$

Figure 10. Chemical and molecular graph of theaflavin with edge partitions.

By the definition of $RG_{ISI_{(p,q)}}(TH)$, we have

$$RG_{ISI_{(p,q)}}(TH) = \sum_{uv \in E(TH)} [\Phi_u \Phi_v]^p [\Phi_u + \Phi_v]^q$$

$$RG_{ISI_{(p,q)}}(TH) = \sum_{uv \in E_1(TH)} [\Phi_u \Phi_v]^p [\Phi_u + \Phi_v]^q + \sum_{uv \in E_2(TH)} [\Phi_u \Phi_v]^p [\Phi_u + \Phi_v]^q + \sum_{uv \in E_3(TH)} [\Phi_u \Phi_v]^p [\Phi_u + \Phi_v]^q$$

$$= |E_1(A)|[(1)(1)]^p[1+1]^q + |E_2(A)|[(1)(2)]^p[1+2]^q + |E_3(A)|[(1)(3)]^p[1+3]^q$$

$$= (14)[1]^p[2]^q + (22)[2]^p[3]^q + (10)[3]^p[4]^q$$

Hence the theorem.

From theorem 10 we have some reverse degree-based indices of theaflavin as below:

(i). $RG_{ISI_{(0,1)}} = RM_1(TH) = 134$

(ii). $RG_{ISI_{(1,0)}} = RM_2(TH) = 88$

(iii). $RG_{ISI_{(\frac{-1}{2},0)}} = RR(TH) = 35.32985187$

(iv). $RG_{ISI_{(0,\frac{-1}{2})}} = RSCI(TH) = 27.60120085$

(v). $2RG_{ISI_{(0,-1)}} = RH(TH) = 33.66666667$

(vi). $RG_{ISI_{(0,2)}} = RHZ(TH) = 414$

(vii). $2RG_{ISI_{(\frac{1}{2},-1)}} = RGA(TH) = 43.40205295$

(viii). $\frac{1}{2}RG_{ISI_{(\frac{-1}{2},1)}} = RAG(TH) = 38.88152916$

(ix). $RG_{ISI_{(1,-1)}} = RISI(TH) = 29.16666667$

(x). $RG_{ISI_{(-1,1)}} = RReZG_1(TH) = 54.33333333$

(xi). $RG_{ISI_{(1,1)}} = RReZG_3(TH) = 260$

3.1. Reverse degree-based Quantitative Structure-Property Relationship (QSPR) analysis.

We evaluate the efficacy of reverse degree-based topological indices by developing a quantitative structure-property relationship (QSPR) between several reverse degree-based topological indices and certain physicochemical properties of potential COVID-19 drugs. Arbidol, Camostat, Chloroquine, Hydroxychloroquine, Lopinavir, Nafamostat, Remdesivir, Ritonavir, Thalidomide, Theaflavin were selected for this analysis, and their physicochemical properties (Table 2) such as Boiling Point (BP), Enthalpy of Vaporization (E), Flash Point (FP), Molar Refractivity (MR), Polar Surface Area (PSA), Polarizability (P), Surface Tension (T) and Molar Volume (MV) were collected from ChemSpider and [30].

Table 2. The physicochemical properties of some COVID-19 drugs.

Drugs	Boiling Point (BP)	Enthalpy of Vaporization: (E)	Flash Point: (FP)	Molar Refractivity (MR)	Polar Surface Area (PSA)	Polarizability (P)	Surface Tension (T)	Molar Volume (MV)
Arbidol	591.8	91.5	311.7	121.9	80	48.3	45.3	347.3
Camostat	634.6	93.8	337.6	105.4	137	41.8	50.6	309.5
Chloroquine	460.6	72.1	232.3	97.4	28	38.6	44.0	287.9
Hydroxychloroquine	516.7	83.0	266.3	99.0	48	39.2	49.8	285.4
Lopinavir	924.2	140.8	512.7	179.2	120	71.0	49.5	540.5
Nafamostat	637.2	94.1	339.1	95.4	141	37.8	61.9	248.4
Remdesivir	-	-	-	149.5	213	59.3	62.3	409
Ritonavir	947.0	144.4	526.6	198.9	202	78.9	53.7	581.7
Thalidomide	487.8	79.4	248.8	65.2	87	25.9	71.6	161
Theaflavin	1003.9	153.5	336.5	137.3	218	54.4	138.6	301.0

Table 3. Reverse degree indices for some COVID-19 drugs.

Drugs	RM_1	RM_2	$RR_{\frac{1}{2}}$	$RSCI$	RH	RHZ	RGA	RAG	$RISI$	$RReZG_1$	$RReZG_3$
Arbidol	98	75	22.23631094	18.00732705	21.40	334	29.66122969	32.49476550	22.20	46.33	270
Camostat	100	75	19.85516038	16.65181787	18.67	344	28.14712250	32.05346651	21.92	42.33	264
Chloroquine	78	64	14.95647849	12.73684398	14.30	278	22.00535110	24.07856459	17.90	31.33	240

Drugs	RM_1	RM_2	$RR_{\frac{1}{2}}$	$RSCI$	RH	RHZ	RGA	RAG	$RISI$	$RReZG_1$	$RReZG_3$
Hydroxy-chloroquine	82	68	15.45647849	13.23684398	14.80	294	23.00535110	25.07856459	18.90	32.33	256
Lopinavir	162	127	32.76093778	27.49675286	31.33	560	46.78438405	51.45080774	36.83	68.67	454
Nafamostat	90	66	19.20045985	15.85892465	18.167	300	26.41507169	29.74406543	19.92	40.67	226
Remdesivir	230	288	19.15023333	20.21227396	18.36	1220	43.41616283	46.76790298	53.99	40.083	1586
Ritonavir	176	136	35.08092873	29.54664090	33.33	606	50.30726371	55.96946931	39.58	74	482
Thalidomide	64	47	15.55204177	12.41384908	15	210	20.12095587	21.98276318	14.50	32.33	162
Theaflavin	134	88	35.32985187	27.60120085	33.67	414	43.40205295	38.88152916	29.17	54.33	260

Eleven reverse degree-based topological indices such as reverse first. Second Zagreb index, reverse Randić index, reverse sum connectivity index, reverse harmonic index, reverse hyper Zagreb index, reverse geometric-arithmetic index, reverse arithmetic-geometric index, reverse inverse sum indeg index, reverse redefined first Zagreb index and reverse redefined third Zagreb index that was examined in this section (Table 3). To conduct prediction analyses, we examine the following linear regression model. $P_p = m\left(RG_{ISI_{(p,q)}}\right) + d,$

Where P_p is any physical property from table 1, d is the regression model constant, m is the individual reverse degree-based topological indices coefficient, and $RG_{ISI_{(p,q)}}$ is any predictor from table 3. This linear regression model was used in compiling table 4, which shows a correlation coefficient of the physicochemical properties of ten COVID 19 drugs and investigating reverse degree-based topological indices, using data from tables 2, 3, and SPSS software. Our linear regression models listed in Table 5 are based on the highest correlation coefficients in Table 4, written in bold, to predict each physicochemical property of the studied drugs. As indicated in Table 5, r stands for correlation coefficient, SE represents a standard error, and F represents F statistics. An illustration of this situation can be seen in Figure 11-17 graphically. Using both correlation (Table 4) and regression analyses (Table 5), we can conclude that the most predictive reverse degree-based topographic indices are

- $RG_{ISI_{(\frac{-1}{2},0)}} = RR(G)$ (reverse Randić index) for *BP* (Boiling point) & Enthalpy of vaporization (*E*).
- $\frac{1}{2}RG_{ISI_{(\frac{-1}{2},1)}} = RAG(G)$ (reverse arithmetic-geometric index) for *FP* (Flashpoint), *MR* (Molar refractivity), *MV* (Molar volume), and *P* (Polarizability).
- $2RG_{ISI_{(\frac{1}{2},-1)}} = RGA(G)$ (reverse geometric arithmetic index) for *PSA* (Polar surface area).

Table 4. Correlations between reverse topological indices and physicochemical properties of COVID-19 drugs.

	RM_1	RM_2	$RR_{\frac{1}{2}}$	$RSCI$	RH	RHZ	RGA	RAG	$RISI$	$RReZG_1$	$RReZG_3$
Boiling Point (BP)	0.921693326	0.83153354	**0.984957973**	0.97934052	0.982810162	0.865844307	0.962800986	0.8850942	0.903172718	0.901332556	0.71518039
Enthalpy of Vaporization: (E)	0.917821994	0.828941645	**0.987248753**	0.980158209	0.986236282	0.861410328	0.962531641	0.8787326	0.901178039	0.8967595	0.7128015
Flash Point: (FP)	0.942886513	0.955618991	0.819850243	0.864192451	0.817047475	0.95688888	0.902012996	**0.9722246**	0.947551476	0.9611071	0.9366844
Molar Refractivity (MR)	0.81606386	0.575442959	0.820976339	0.911122553	0.821706812	0.597639576	0.951552475	**0.9733115**	0.795621021	0.9037533	0.4259689
Molar Volume (MV)	0.749150694	0.534693133	0.700687639	0.799927439	0.70116223	0.550802546	0.85535017	**0.9283629**	0.735957625	0.8617609	0.3948805
Polar Surface Area (PSA)	0.754479093	0.607555724	0.649979029	0.729899954	0.645243941	0.636082394	**0.782495012**	0.7144299	0.72531629	0.5598402	0.5199564
Polarizability (P)	0.816550807	0.576092838	0.820725436	0.911039333	0.82144982	0.598285248	0.951685154	**0.9735999**	0.796122829	0.9037271	0.4266732
Surface Tension(T)	0.103670046	-0.016192078	0.450800976	0.377518315	**0.451245573**	0.008247485	0.274693946	0.0609114	0.07168639	0.1202036	-0.0543605

Table 5. Statistically best linear prediction models.

Regression Equation	***r***	**SE**	***F***
$BP = 123.542 + 24.198(RR_{\frac{1}{2}})$	0.984957973	39.10265	227.445
$E = 22.043 + 3.584(RR_{\frac{1}{2}})$	0.987248753	5.32331	269.244
$MR = 4.057 + 3.371(RAG)$	0.973311517	10.07987	143.904
$P = 1.586 + 1.337(RAG)$	0.973599989	3.97506	145.542

Regression Equation	*r*	SE	*F*
$FP = 47.486 + 8.611(RAG)$	0.972224608	26.61489	120.785
$MV = -14.009 + 10.075(RAG)$	0.928362855	51.14717	49.911
$PSA = -27.912 + 4.660(RGA)$	0.782495012	44.84448	12.634

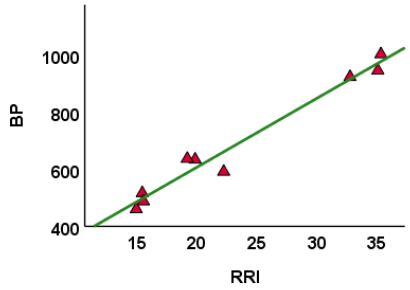

Figure 11. Reverse Randic index versus Boiling Point.

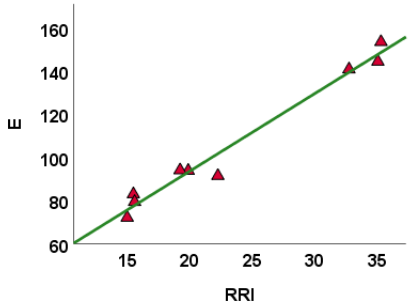

Figure 12. Reverse Randic index versus Enthalpy of Vaporization

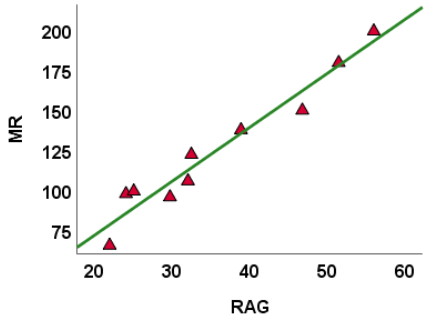

Figure 13. Reverse Arithmetic Geometric index versus Molar Refractivity.

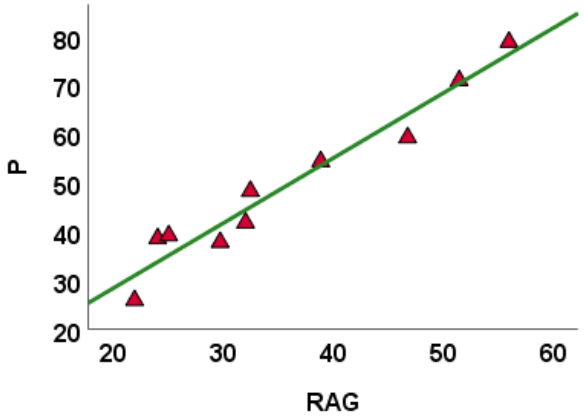

Figure-14. Reverse Arithmetic Geometric index versus Polarizability.

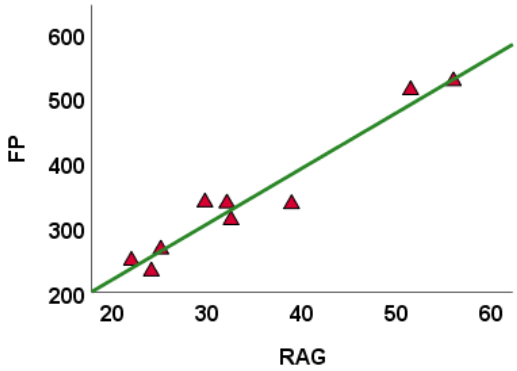

Figure 15. Reverse Arithmetic Geometric index versus Flash Point.

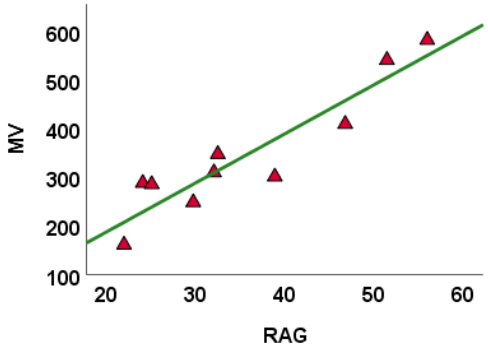

Figure 16. Reverse Arithmetic Geometric index versus Molar Volume.

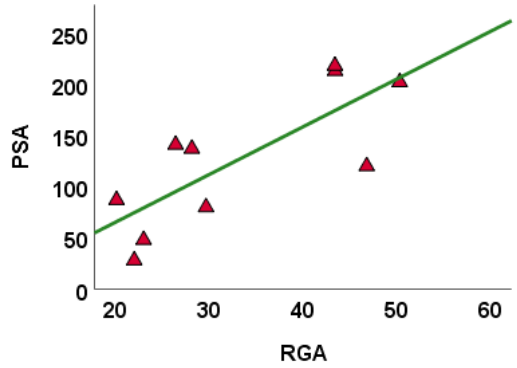

Figure 17. Reverse Geometric Arithmetic index versus Polar Surface Area.

4. Conclusions

Drug development can be aided by topological indices, which allow insights into the molecular structure of the molecule. So in this article, by using reverse degree topological indices, we examined the molecular structure of certain antiviral drugs used to treat COVID-19. We first computed the general reverse inverse sum indeg index for ten antiviral drugs, then derived several reverse topological indices. Next, in this article, we tried to verify whether reverse degree-based topological indices had any meaningful interpretation and, more specifically, if they could be incorporated into QSPR models. Based on a QSPR analysis, we found topological indices based on reverse degrees to be extremely effective for predicting the physicochemical properties of studied drugs. The most predictive reverse degree topological indices are Reverse Randić index (RAG) for *BP* (Boiling point) & Enthalpy of vaporization (E), Reverse arithmetic-geometric index (RAG) for *FP* (Flash point), *MR* (Molar refractivity),

MV (Molar volume), *P* (Polarizability) and Reverse geometric arithmetic index (*RGA*) for *PSA* (Polar surface area).

Funding

This research received no external funding.

Acknowledgments

This research has no acknowledgment.

Conflicts of Interest

The authors declare no conflict of interest.

References

1. Christian, M.D.; Poutanen, S.M.; Loutfy, M.R.; Muller, M.P.; Low, D.E. Severe Acute Respiratory Syndrome. *Clinical Infectious Diseases* **2004**, *38*, 1420-1427, https://doi.org/10.1086/420743.
2. Girard, M.P.; Tam, J.S.; Assossou, O.M.; Kieny, M.P. The 2009 A (H1N1) influenza virus pandemic: A review. *Vaccine* **2010**, *28*, 4895-4902, https://doi.org/10.1016/j.vaccine.2010.05.031.
3. Z Zumla, A.; Hui, D.S.; Perlman, S. Middle East respiratory syndrome. *The Lancet* **2015**, *386*, 995-1007, https://doi.org/10.1016/S0140-6736(15)60454-8.
4. Oleribe, O.O.; Salako, B.L.; Ka, M.M.; Akpalu, A.; McConnochie, M.; Foster, M.; Taylor-Robinson, S.D. Ebola virus disease epidemic in West Africa: lessons learned and issues arising from West African countries. *Clinical Medicine* **2015**, *15*, https://doi.org/10.7861/clinmedicine.15-1-54.
5. Agumadu, V.C.; Ramphul, K. Zika virus: a review of literature. *Cureus* **2018**, *10*, https://doi.org/10.7759/cureus.3025.
6. Wu, F.; Zhao, S.; Yu, B.; Chen, Y.-M.; Wang, W.; Song, Z.-G.; Hu, Y.; Tao, Z.-W.; Tian, J.-H.; Pei, Y.-Y. A new coronavirus associated with human respiratory disease in China. *Nature* **2020**, *579*, 265-269, https://doi.org/10.1038/s41586-020-2008-3.
7. Chung, Y.H.; Beiss, V.; Fiering, S.N.; Steinmetz, N.F. COVID-19 Vaccine Frontrunners and Their Nanotechnology Design. *ACS Nano* **2020**, *14*, 12522-12537, https://doi.org/10.1021/acsnano.0c07197.
8. Carvalho, T. COVID-19 Research in Brief: 9 May to 15 May, 2020. Nature medicine **2020.** https://doi.org/10.1038/d41591-020-00018-w.
9. Lung, J.; Lin, Y.-S.; Yang, Y.-H.; Chou, Y.-L.; Shu, L.-H.; Cheng, Y.-C.; Liu, H.T.; Wu, C.-Y. The potential chemical structure of anti-SARS-CoV-2 RNA-dependent RNA polymerase. *Journal of Medical Virology* **2020**, *92*, 693-697, https://doi.org/10.1002/jmv.25761.
10. Dolnicar, S.; Chapple, A. The readability of articles in tourism journals. *Annals of Tourism Research* **2015**, *52*, 161-166, https://doi.org/10.1016/j.annals.2015.03.003.
11. Takahashi, W.; Yoneda, T.; Koba, H.; Ueda, T.; Tsuji, N.; Ogawa, H.; Asakura, H. Potential mechanisms of nafamostat therapy for severe COVID-19 pneumonia with disseminated intravascular coagulation. *Int J Infect Dis* **2021**, *102*, 529-531.
12. Breining, P.; Frølund, A.L.; Højen, J.F.; Gunst, J.D.; Staerke, N.B.; Saedder, E.; Cases-Thomas, M.; Little, P.; Nielsen, L.P.; Søgaard, O.S. Camostat mesylate against SARS-CoV-2 and COVID-19—Rationale, dosing and safety. *Basic & Clinical Pharmacology & Toxicology* **2021**, *128*, 204-212, https://doi.org/10.1111/bcpt.13533.
13. Luo, L.; Qiu, Q.; Huang, F.; Liu, K.; Lan, Y.; Li, X.; Huang, Y.; Cui, L.; Luo, H. Drug repurposing against coronavirus disease 2019 (COVID-19): A review. *Journal of Pharmaceutical Analysis* **2021**, *11*, 683-690, https://doi.org/10.1016/j.jpha.2021.09.001.
14. Ali, A.S.; Ibrahim, I.M.; Burzangi, A.S.; Ghoneim, R.H.; Aljohani, H.S.; Alsamhan, H.A.; Barakat, J. Scoping insight on antiviral drugs against COVID-19. *Arabian Journal of Chemistry* **2021**, *14*, https://doi.org/10.1016/j.arabjc.2021.103385.
15. Iwanami, S.; Ejima, K.; Kim, K.S.; Noshita, K.; Fujita, Y.; Miyazaki, T.; Kohno, S.; Miyazaki, Y.; Morimoto, S.; Nakaoka, S. Detection of significant antiviral drug effects on COVID-19 with reasonable sample sizes in randomized controlled trials: A modeling study. *PLOS Medicine* **2021**, *18*, https://doi.org/10.1371/journal.pmed.1003660.
16. Roy, K.; Kar, S.; Das, R.N. *A primer on QSAR/QSPR modeling: fundamental concepts*. Springer, **2015**; https://doi.org/10.1007/978-3-319-17281-1.

17. Castro, E.A. QSPR-QSAR studies on desired properties for drug design. Research Signpost: Kerala, India **2010.**
18. Estrada, E.; Patlewicz, G.; Uriarte, E. From molecular graphs to drugs. A review on the use of topological indices in drug design and discovery. *NISCAIR-CSIR, India* **2003**.
19. Todeschini, R.; Consonni, V. *Handbook of molecular descriptors*. John Wiley & Sons, Volume 11, **2008.**
20. Roy, K. *Advances in QSAR modeling. Applications in pharmaceutical, chemical, food, agricultural and environmental sciences.* Springer, Cham **2017**; pp. 555, https://doi.org/10.1007/978-3-319-56850-8.
21. Mauri, A.; Consonni, V.; Todeschini, R. Molecular Descriptors. In: *Handbook of Computational Chemistry.* Leszczynski, J. Ed.; Springer Netherlands: Dordrecht, **2016**; pp. 1–29, https://doi.org/10.1007/978-94-007-6169-8_51-1.
22. Dearden, J.C. The use of topological indices in QSAR and QSPR modeling. In: *Advances in QSAR modeling*. Springer, **2017**; pp. 57–88, https://doi.org/10.1007/978-3-319-56850-8_2.
23. Wiener, H. Structural determination of paraffin boiling points. *Journal of the American Chemical Society* **1947**, *69*, 17–20, https://doi.org/10.1021/ja01193a005.
24. Wiener, H. Correlation of heats of isomerization, and differences in heats of vaporization of isomers, among the paraffin hydrocarbons. *Journal of the American Chemical Society* **1947**, *69*, 2636–2638, https://doi.org/10.1021/ja01203a022.
25. Gutman, I.; Trinajstić, N. Graph theory and molecular orbitals. Total φ-electron energy of alternant hydrocarbons. *Chemical Physics Letters* **1972,** *17*, 535–538.
26. Randic, M. Characterization of molecular branching. *Journal of the American Chemical Society* **1975**, *97*, 6609–6615, https://doi.org/10.1021/ja00856a001.
27. Gutman, I.; Milovanović, E.; Milovanović, I. Beyond the Zagreb indices. *AKCE International Journal of Graphs and Combinatorics* **2020**, *17*, 74-85, https://doi.org/10.1016/j.akcej.2018.05.002.
28. Gutman, I.; Tošović, J. Testing the quality of molecular structure descriptors. Vertex-degree-based topological indices. *Journal of the Serbian Chemical Society* **2013,** *78*, 805–810, https://doi.org/10.2298/JSC121002134G.
29. Zhong, J.-F.; Rauf, A.; Naeem, M.; Rahman, J.; Aslam, A. Quantitative structure-property relationships (QSPR) of valency based topological indices with Covid-19 drugs and application. *Arabian Journal of Chemistry* **2021**, *14*, https://doi.org/10.1016/j.arabjc.2021.103240.
30. Kirmani, S.A.K.; Ali, P.; Azam, F. Topological indices and QSPR/QSAR analysis of some antiviral drugs being investigated for the treatment of COVID-19 patients. *International Journal of Quantum Chemistry* **2021**, *121*, https://doi.org/10.1002/qua.26594.
31. Havare, Ö.Ç. Quantitative Structure Analysis of Some Molecules in Drugs Used in the Treatment of COVID-19 with Topological Indices. *Polycyclic Aromatic Compounds* **2021**, 1-12, https://doi.org/10.1080/10406638.2021.1934045.
32. Rosary, M.S. Topological Study of Line Graph of Remdesivir Compound Used in the Treatment of Corona Virus. *Polycyclic Aromatic Compounds* **2021**, 1-17, https://doi.org/10.1080/10406638.2021.1956552.
33. Liu, J.-B.; Singaraj, R.M. Topological analysis of para-line graph of Remdesivir used in the prevention of corona virus. *International Journal of Quantum Chemistry* **2021**, *121*, https://doi.org/10.1002/qua.26778.
34. Ahmed, H.; Alwardi, A.; Salestina, M.R.; Nandappa, D.S. Domination, gamma-Domination Topological Indices and phi (P)-Polynomial of Some Chemical Structures Applied for the Treatment of COVID-19 Patients. *Biointerface Research in Applied Chemistry* **2021**, *11*, 13290–13302, https://doi.org/10.33263/BRIAC115.1329013302.
35. Jahanbani, A. Results about Molecular Structure of Chloroquine and Hydroxychloroquine for the Treatment Coronavirus. *Polycyclic Aromatic Compounds* **2021**, 1-14, https://doi.org/10.1080/10406638.2021.1934047.
36. Mondal, S.; De, N.; Pal, A.; Gao, W. Molecular descriptors of some chemicals that prevent COVID-19. *Current organic synthesis* **2020,** *18*, 729-741, https://doi.org/10.2174/1570179417666201208114509.
37. Mondal, S.; De, N.; Pal, A. Topological Indices of Some Chemical Structures Applied for the Treatment of COVID-19 Patients. *Polycyclic Aromatic Compounds* **2020**, 1-15, https://doi.org/10.1080/10406638.2020.1770306.
38. Liu, J.-B.; Arockiaraj, M.; Arulperumjothi, M.; Prabhu, S. Distance based and bond additive topological indices of certain repurposed antiviral drug compounds tested for treating COVID-19. *International Journal of Quantum Chemistry* **2021**, *121*, https://doi.org/10.1002/qua.26617.
39. Wei, J.; Cancan, M.; Rehman, A.U.; Siddiqui, M.K.; Nasir, M.; Younas, M.T.; Hanif, M.F. On Topological Indices of Remdesivir Compound Used in Treatment of Corona Virus (COVID 19). *Polycyclic Aromatic Compounds* **2021**, 1-19, https://doi.org/10.1080/10406638.2021.1887299.
40. Kulli, V.R. On the sum connectivity reverse index of oxide and honeycomb networks. *Journal of Computer and Mathematical Sciences* **2017**, *8*, 408–413.